Electronic Supporting Information

Photoluminescent Lanthanide-Organic Bilayer Networks with 2,3-Pyrazinedicarboxylate and Oxalate

Paula C. R. Soares-Santos [a,b], Luís Cunha-Silva [a,c], Filipe A. Almeida Paz [a], Rute A. S. Ferreira [b], João Rocha [a], Luís D. Carlos *[,b], Helena I. S. Nogueira *[,a]

A contribution from

CICECO, Departments of Chemistry[a] and Physics[b], University of Aveiro, 3810-193 Aveiro, Portugal

REQUIMTE & Department of Chemistry[c], Faculty of Sciences, University of Porto, Rua do Campo Alegre, 4169-007 Porto, Portugal

Table S1

Table S1. Selected bond lengths (in Å) and angles (in degrees) for the coordination Polyhedron of Ce^{3+} in $[Ce_2(2,3\text{-pzdc})_2(ox)(H_2O)_2]_n$ (**1**).[a]

Ce(1)–O(1)	2.483(5)	$O(2)^{i}$–Ce(1)–O(1W)	153.45(15)
Ce(1)–$O(2)^{i}$	2.465(5)	$O(2)^{i}$–Ce(1)–N(1)	75.33(9)
Ce(1)–O(3)	2.419(4)	O(3)–Ce(1)–$O(3)^{ii}$	73.2(2)
Ce(1)–$O(3)^{ii}$	2.419(4)	O(3)–Ce(1)–$O(4)^{iii}$	100.01(14)
Ce(1)–$O(4)^{iii}$	2.412(3)	O(3)–Ce(1)–$O(4)^{iv}$	147.98(13)
Ce(1)–$O(4)^{iv}$	2.412(3)	O(3)–Ce(1)–O(1W)	70.98(12)
Ce(1)–O(1W)	2.581(5)	O(3)–Ce(1)–N(1)	58.48(12)
Ce(1)–N(1)	2.872(4)	O(3)–Ce(1)–$N(1)^{ii}$	126.66(14)
Ce(1)–$N(1)^{ii}$	2.872(4)	$O(3)^{ii}$–Ce(1)–$N(1)^{ii}$	58.48(12)
		$O(4)^{iii}$–Ce(1)–$O(4)^{iv}$	68.80(17)
O(1)–Ce(1)–$O(2)^{i}$	66.06(16)	$O(4)^{iii}$–Ce(1)–O(1W)	77.21(12)
O(1)–Ce(1)–O(3)	77.58(14)	$O(4)^{iii}$–Ce(1)–N(1)	67.65(11)
O(1)–Ce(1)–$O(4)^{iii}$	132.56(12)	$O(4)^{iii}$–Ce(1)–$N(1)^{ii}$	132.87(11)
O(1)–Ce(1)–O(1W)	140.49(16)	$O(4)^{iv}$–Ce(1)–$N(1)^{ii}$	67.65(11)
O(1)–Ce(1)–N(1)	71.51(8)	O(1W)–Ce(1)–N(1)	109.35(8)
$O(2)^{i}$–Ce(1)–O(3)	128.27(11)	N(1)–Ce(1)–$N(1)^{ii}$	139.62(16)
$O(2)^{i}$–Ce(1)–$O(4)^{iii}$	80.95(12)		

[a] Symmetry transformations used to generate equivalent atoms:
(i) *–x+1, –y+1, –z+1*; (ii) *x, –y+1, z*; (iii) *x–½, –y+½, z;* (iv) *x–½, y+½, z*.

Table S2

Table S2. Selected bond lengths (in Å) and angles (in degrees) for the coordination Polyhedron of Tb^{3+} in $[Tb_2(2\text{-pzc})_4(ox)(H_2O)_6]\cdot 10H_2O$ (**8**).[a]

Tb(1)–O(1)	2.485(5)	O(2)^i–Tb(1)–N(1)	139.85(19)
Tb(1)–O(2)^i	2.387(5)	O(2)^i–Tb(1)–N(3)	74.60(18)
Tb(1)–O(3)	2.369(5)	O(3)–Tb(1)–O(5)	133.60(17)
Tb(1)–O(5)	2.326(5)	O(3)–Tb(1)–O(1W)	139.00(18)
Tb(1)–O(1W)	2.451(5)	O(3)–Tb(1)–O(2W)	77.06(19)
Tb(1)–O(2W)	2.409(5)	O(3)–Tb(1)–O(3W)	83.18(18)
Tb(1)–O(3W)	2.413(4)	O(3)–Tb(1)–N(1)	63.19(18)
Tb(1)–N(1)	2.677(6)	O(3)–Tb(1)–N(3)	142.30(18)
Tb(1)–N(3)	2.682(6)	O(5)–Tb(1)–O(1W)	76.30(18)
		O(5)–Tb(1)–O(2W)	92.6(2)
O(1)–Tb(1)–O(2)^i	66.84(17)	O(5)–Tb(1)–O(3W)	77.43(17)
O(1)–Tb(1)–O(3)	72.44(18)	O(5)–Tb(1)–N(1)	70.52(18)
O(1)–Tb(1)–O(5)	132.68(18)	O(5)–Tb(1)–N(3)	63.91(17)
O(1)–Tb(1)–O(1W)	66.79(17)	O(1W)–Tb(1)–O(2W)	137.27(19)
O(1)–Tb(1)–O(2W)	134.63(19)	O(1W)–Tb(1)–O(3W)	77.08(17)
O(1)–Tb(1)–O(3W)	66.53(17)	O(1W)–Tb(1)–N(1)	136.39(18)
O(1)–Tb(1)–N(1)	119.21(18)	O(1W)–Tb(1)–N(3)	70.01(18)
O(1)–Tb(1)–N(3)	123.97(18)	O(2W)–Tb(1)–O(3W)	141.3(2)
O(2)^i–Tb(1)–O(3)	84.48(18)	O(2W)–Tb(1)–N(1)	72.6(2)
O(2)^i–Tb(1)–O(5)	137.93(17)	O(2W)–Tb(1)–N(3)	68.11(18)
O(2)^i–Tb(1)–O(1W)	83.62(18)	O(3W)–Tb(1)–N(1)	68.82(18)
O(2)^i–Tb(1)–O(2W)	77.6(2)	O(3W)–Tb(1)–N(3)	133.66(18)
O(2)^i–Tb(1)–O(3W)	133.35(18)	N(1)–Tb(1)–N(3)	116.57(19)

[a] Symmetry transformations used to generate equivalent atoms: (i) *–x+1, –y+2, –z+2*.

Figure S1

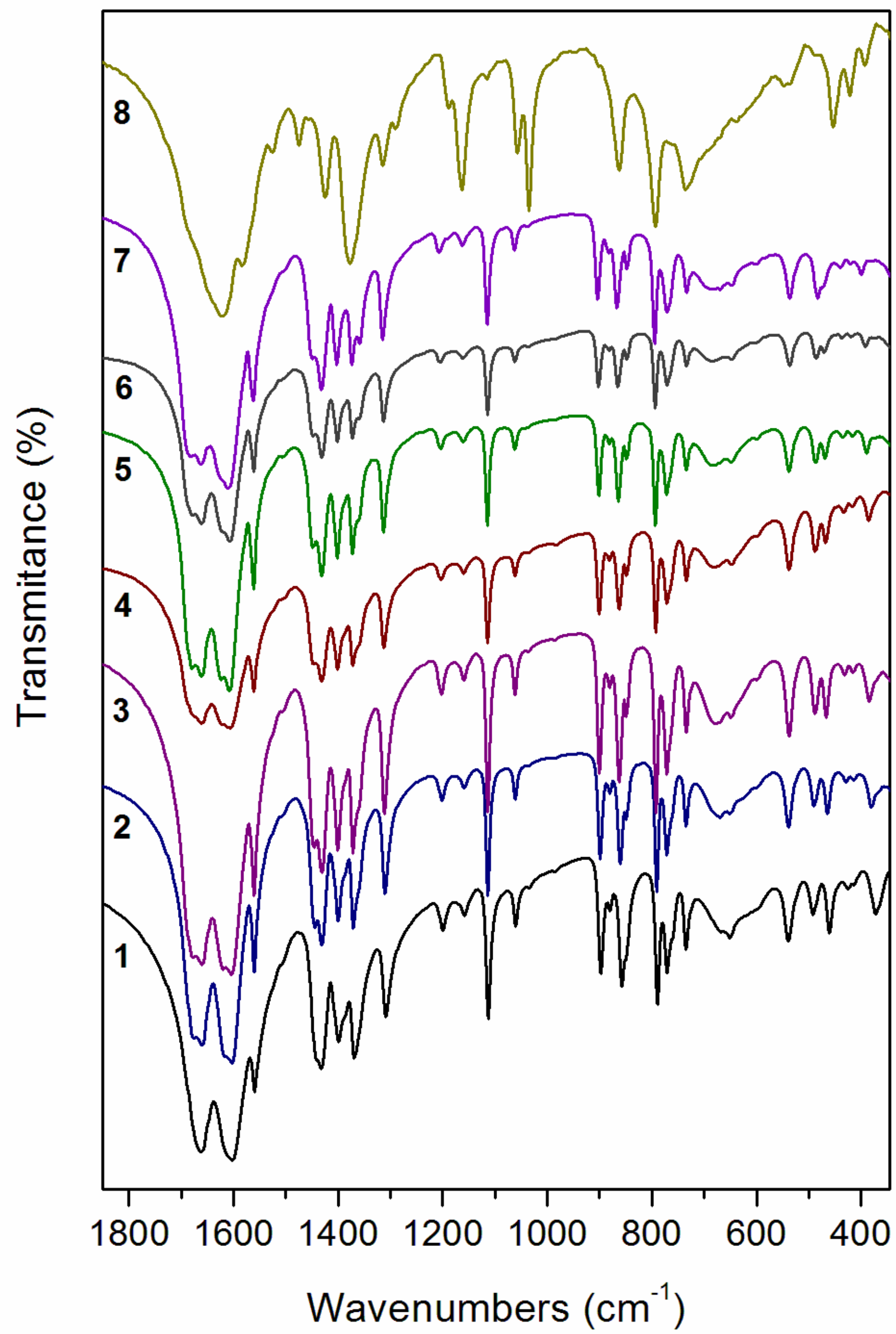

Figure S1. FT-IR spectra of $[Ln_2(2,3\text{-pzdc})_2(ox)(H_2O)_2]_n$ [with Ln(III) = Ce (**1**), Nd (**2**), Sm (**3**), Eu (**4**), Gd (**5**), Tb (**6**) or Er(**7**)] and of $[Tb_2(2\text{-pzc})_4(ox)(H_2O)_6]\cdot 10H_2O$ (**8**).

Figure S2

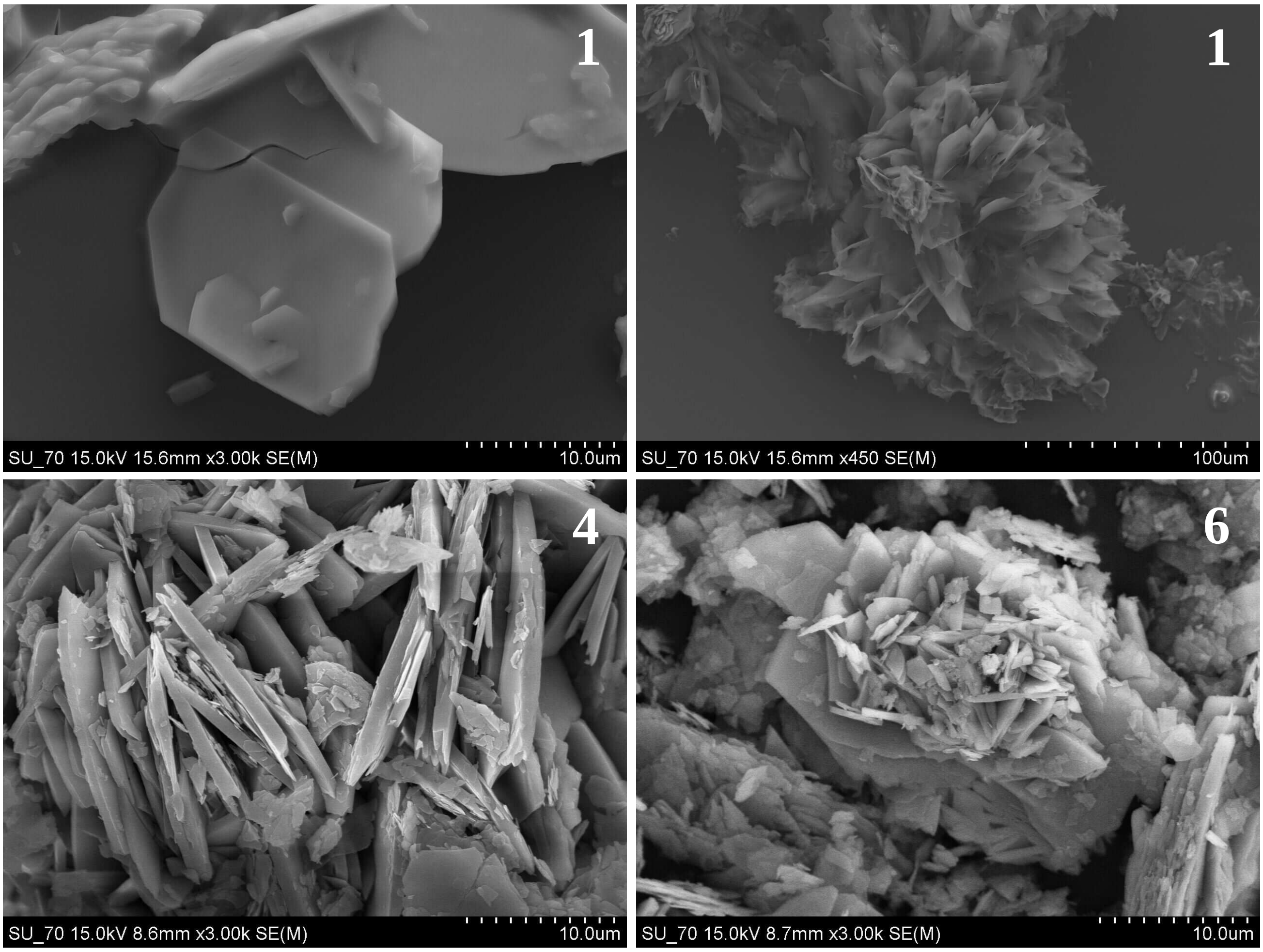

Figure S2. SEM images of $[Ln_2(2,3\text{-pzdc})_2(ox)(H_2O)_2]_n$ [with Ln(III) = Ce (**1**), Eu (**4**) or Tb (**6**)].

Figure S3

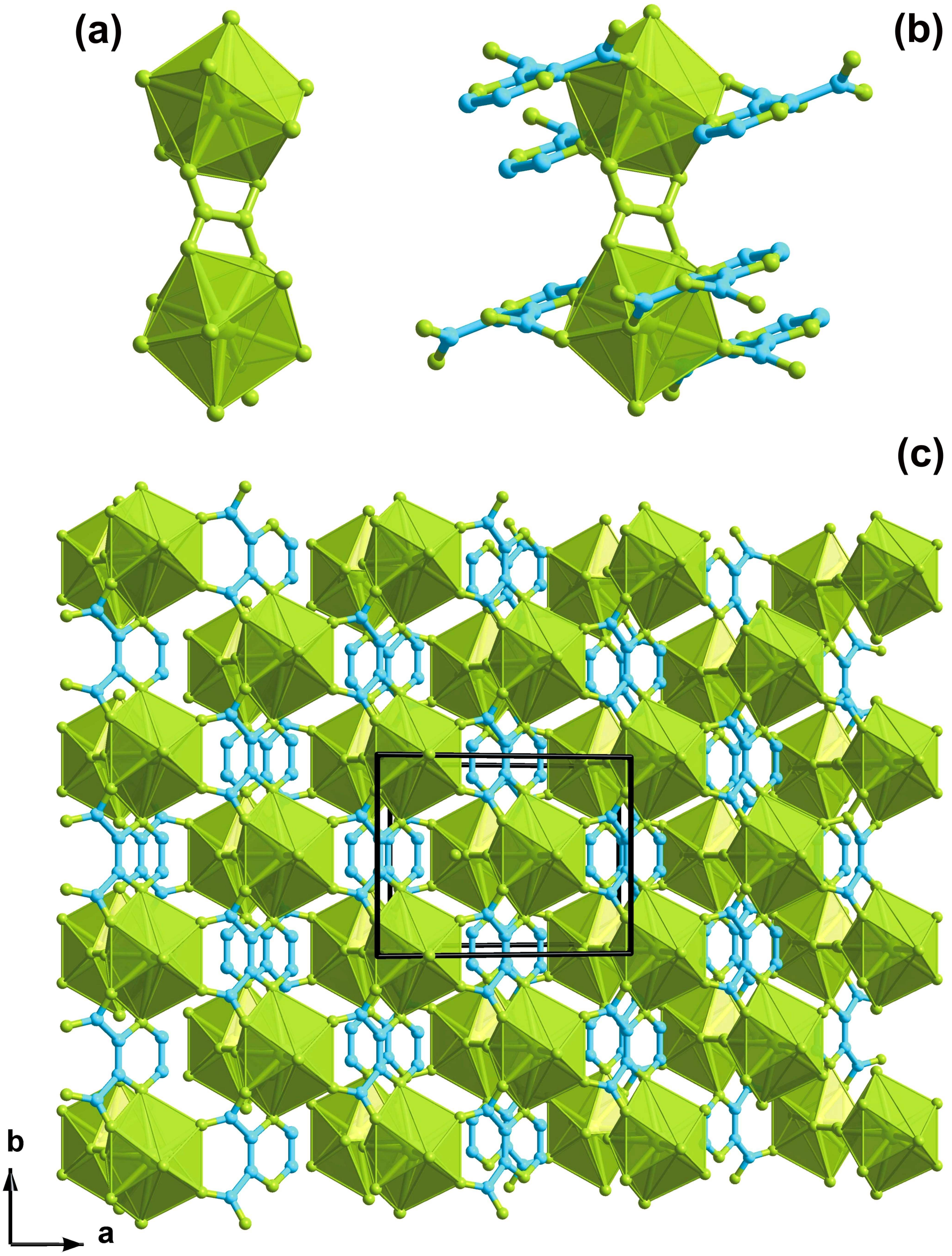

Figure S3. Mixed polyhedral and ball-and-stick representations of the separation between the organic (blue) and the inorganic (green) components in the structure of $[Ce_2(2,3\text{-}pzdc)_2(ox)(H_2O)_2]_n$ (**1**): **(a)** isolated inorganic component (two $\{CeN_2O_4\}$ polyhedra connected by one ox^{2-} anion); **(b)** inorganic part surrounded by six organic components (2,3-$pzdc^{2-}$ ligand); **(c)** $_\infty^{2}[Ce_2(2,3\text{-}pzdc)_2(ox)(H_2O)_2]$ bilayer viewed in perspective along the [001] direction of the unit cell.

Figure S4

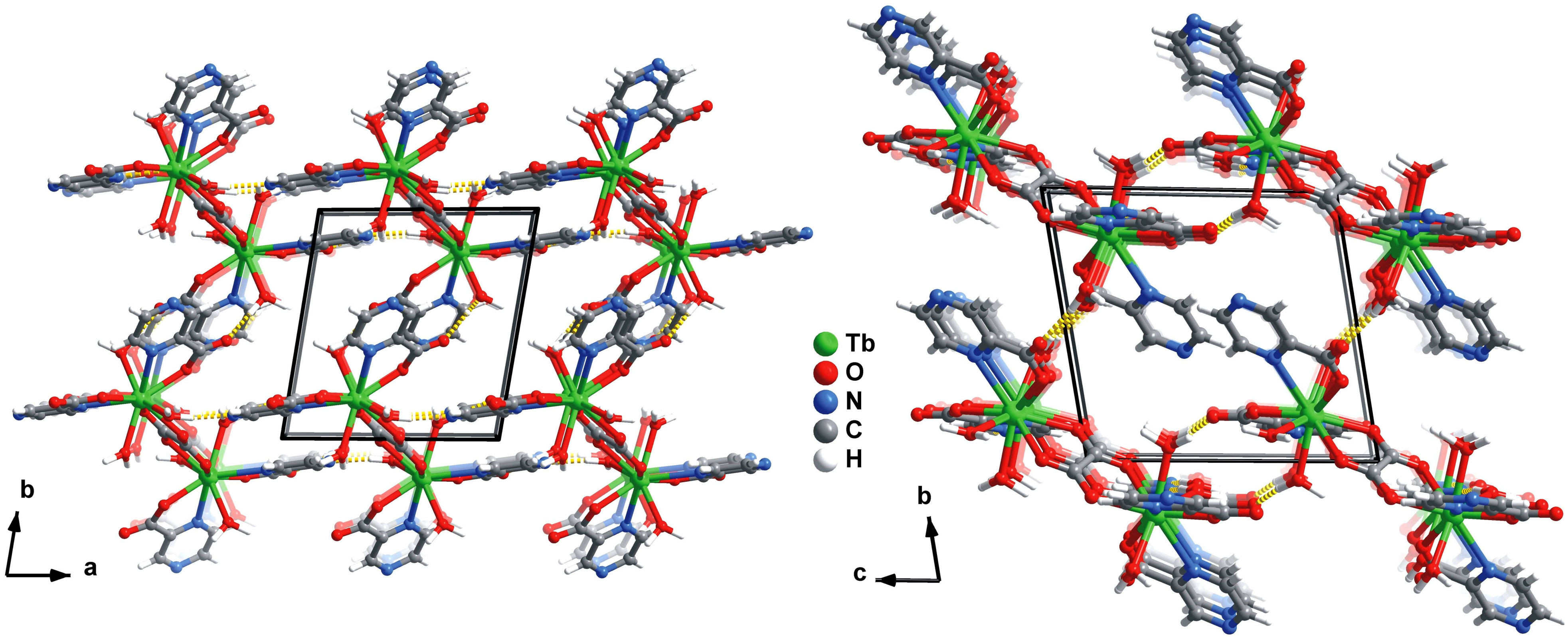

Figure S4. Ball-and-stick representation of the close packing of $[Tb_2(2\text{-pzc})_4(ox)(H_2O)_6]$ complexes viewed in perspective along the **(a)** [001] and **(b)** [100] crystallographic directions, emphasizing the channels running parallel to these directions. Inter-complex hydrogen bonds are drawn as dashed yellow lines. See Table 4 in the main paper for details on the hydrogen bonding geometry.

Figure S5

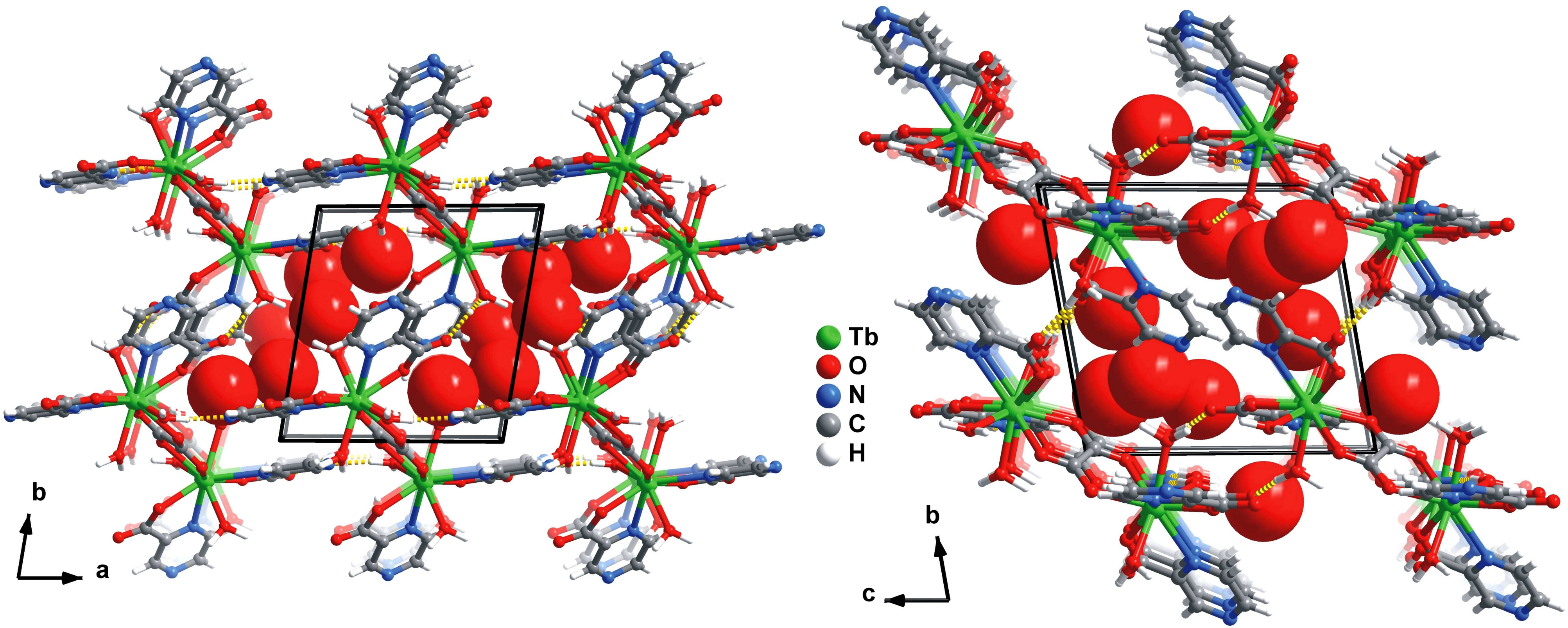

Figure S5. Mixed ball-and-stick and space-filling (crystallization water molecules) representation of the crystal packing of $[Tb_2(2\text{-}pzc)_4(ox)(H_2O)_6]\cdot 10H_2O$ viewed in perspective along the **(a)** [001] and **(b)** [100] crystallographic directions. Channels running parallel to these directions and filled with the uncoordinated crystallization water molecules are emphasized. Inter-complex hydrogen bonds are represented as dashed yellow lines. See Table 4 in the main paper for details on the hydrogen bonding geometry.

Figure S6

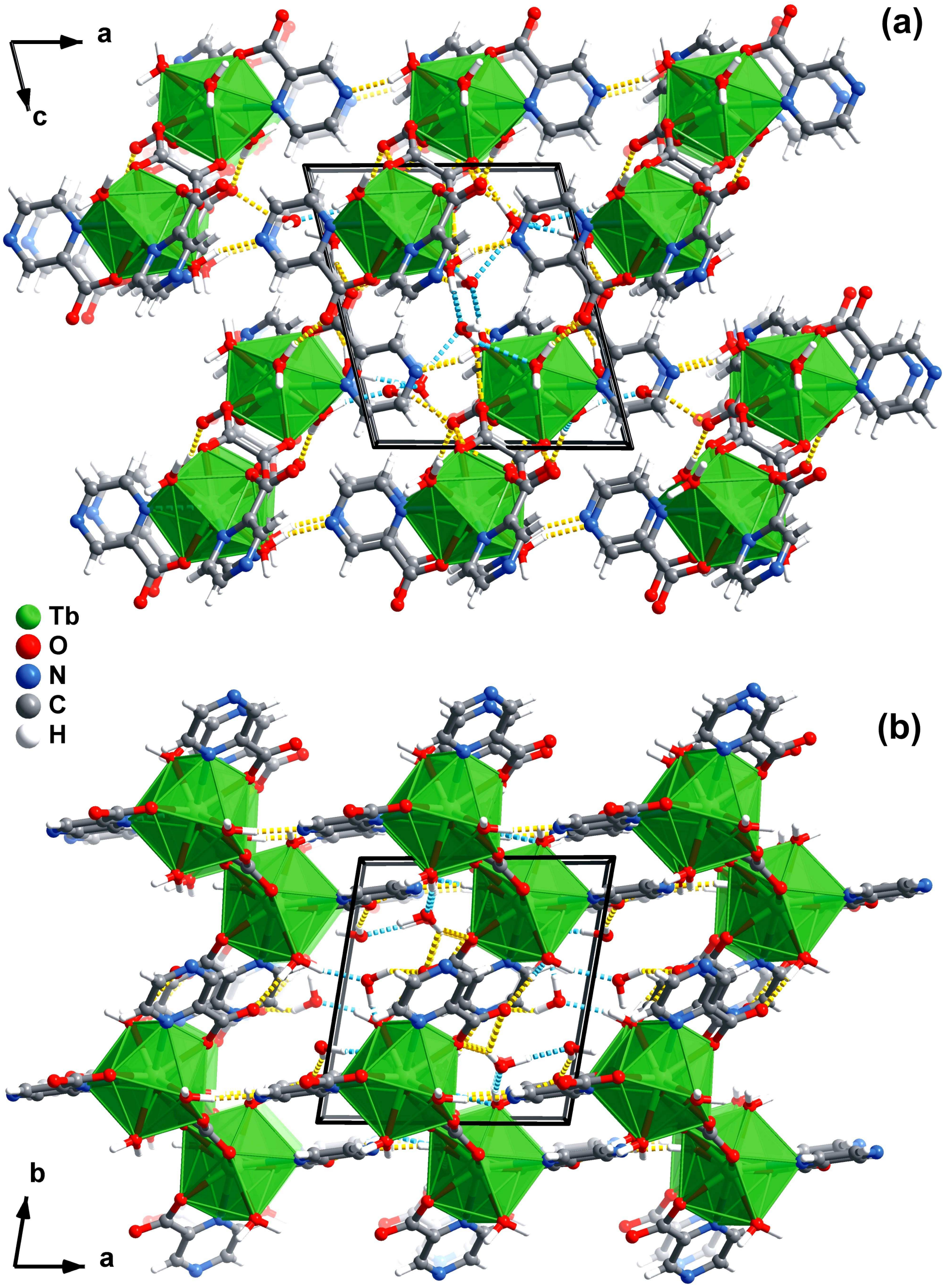

Figure S6. Mixed polyhedral (green) and ball-and-stick representation of the crystal packing of $[Tb_2(2\text{-pzc})_4(ox)(H_2O)_6]\cdot 10H_2O$ viewed in perspective along the **(a)** [010] and **(b)** [001] crystallographic directions. Hydrogen bonds involving the uncoordinated water molecules are represented as dashed blue lines and the remaining hydrogen bonds represented as dashed yellow lines. See Table 4 in the main paper for details on the hydrogen bonding geometry.

Figure S7

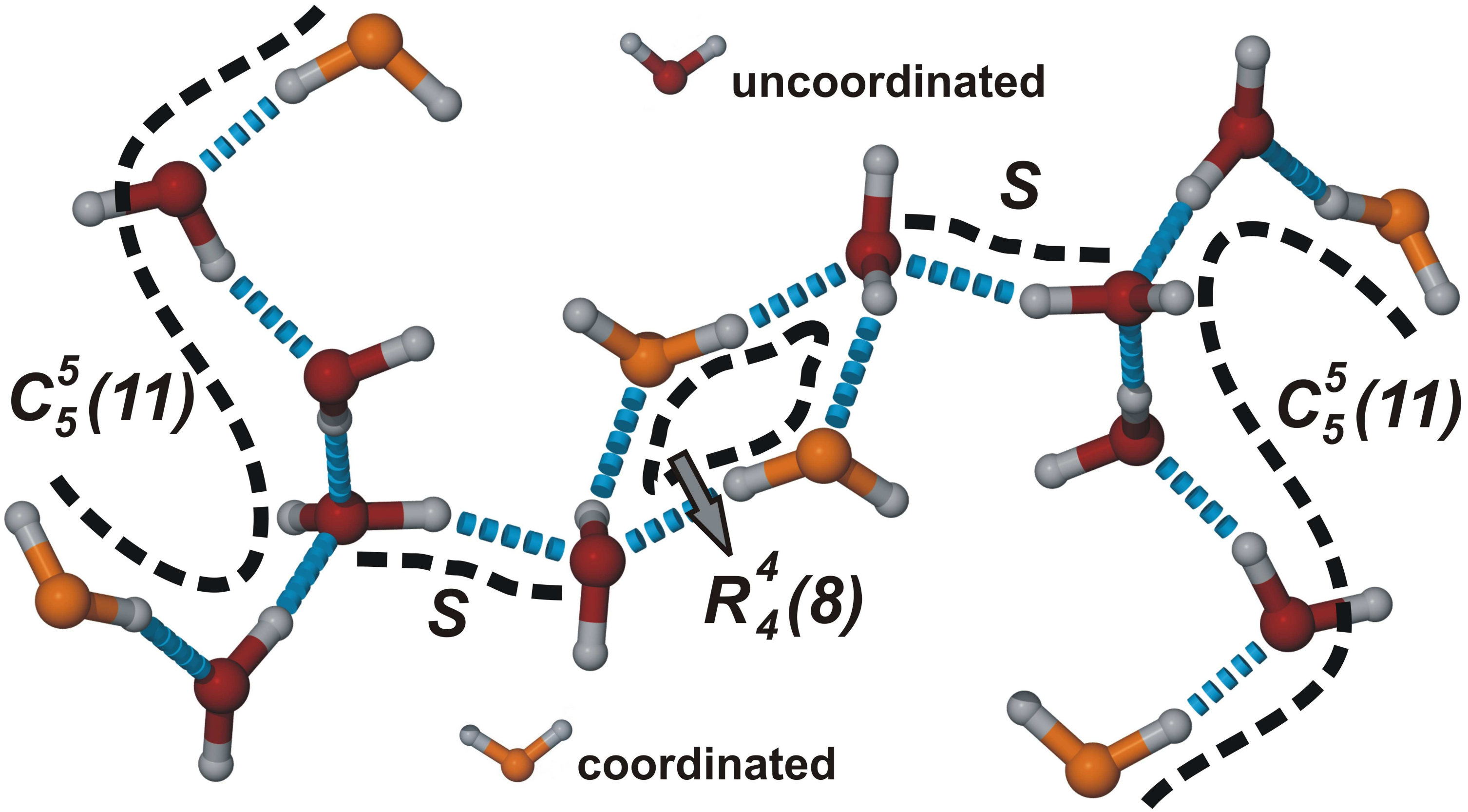

Figure S7. The $(H_2O)_{16}$ cluster that results of a hydrogen bonding network with a graph set motif $[C_5^5(11)]_2(S)_2R_4^4(8)$. Oxygen atoms shown as red and orange represent the uncoordinated and coordinated water molecules, respectively.

Figure S8

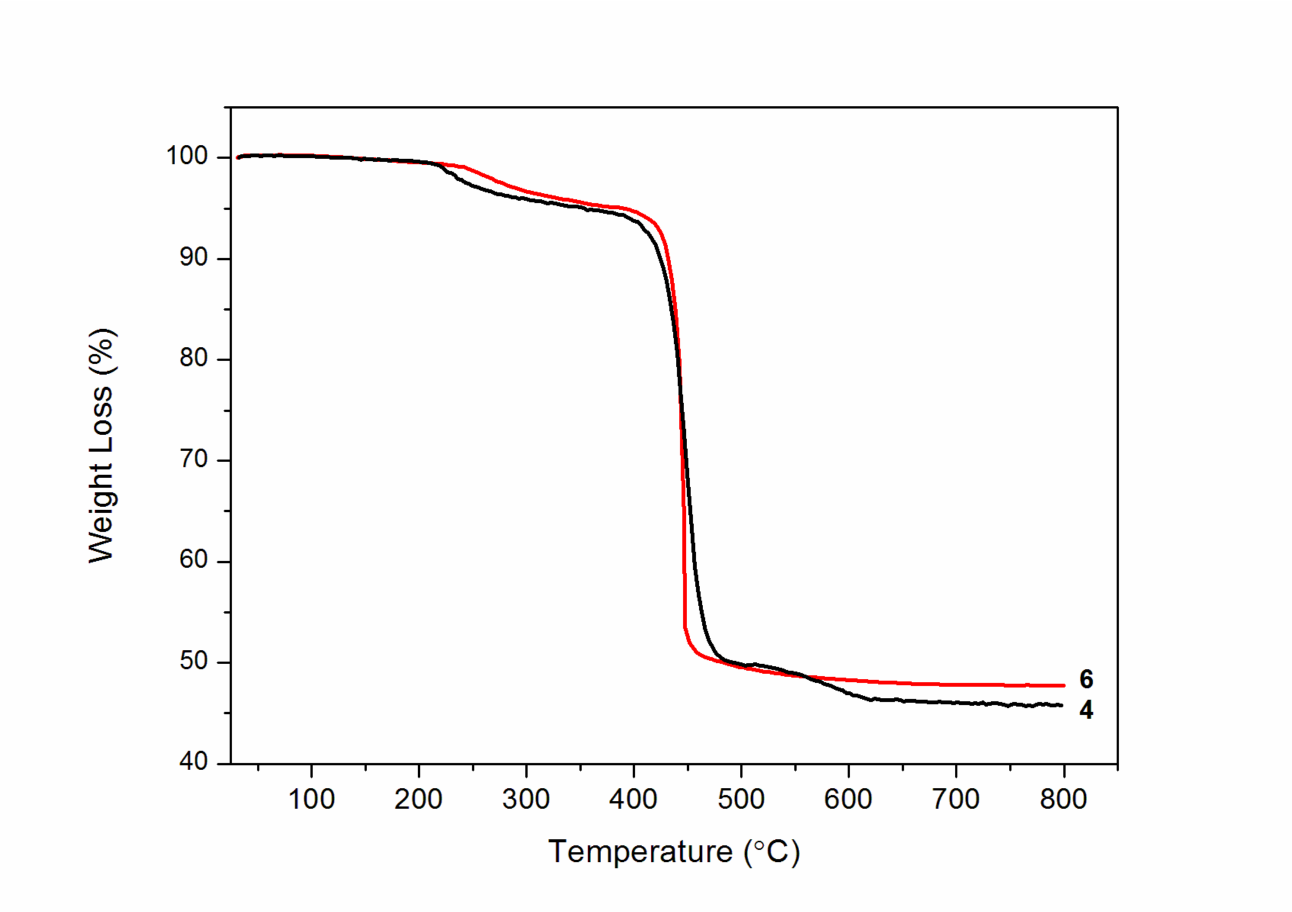

Figure S8. Thermograms for $[Ln_2(2,3\text{-pzdc})_2(ox)(H_2O)_2]_n$ [with Ln(III) = Eu (**4**) or Tb (**6**)].

Figure S9

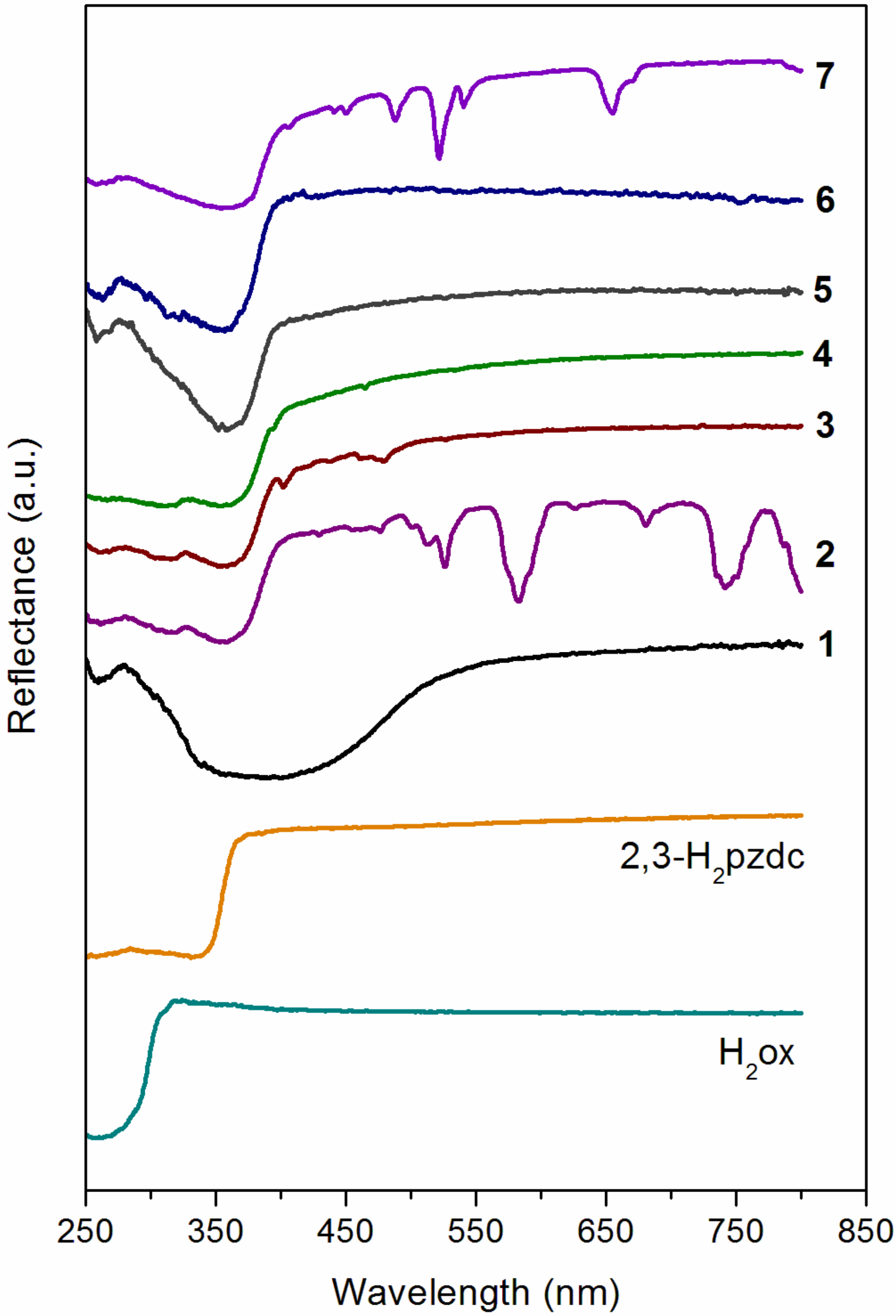

Figure S9. Room temperature diffuse reflectance spectra of free ligands (2,3-H_2pzdc and H_2ox) and of $[Ln_2(2,3\text{-pzdc})_2(ox)(H_2O)_2]_n$ [with Ln(III) = Ce (**1**), Nd (**2**), Sm (**3**), Eu (**4**), Gd (**5**), Tb (**6**) or Er(**7**)].

Figure S10

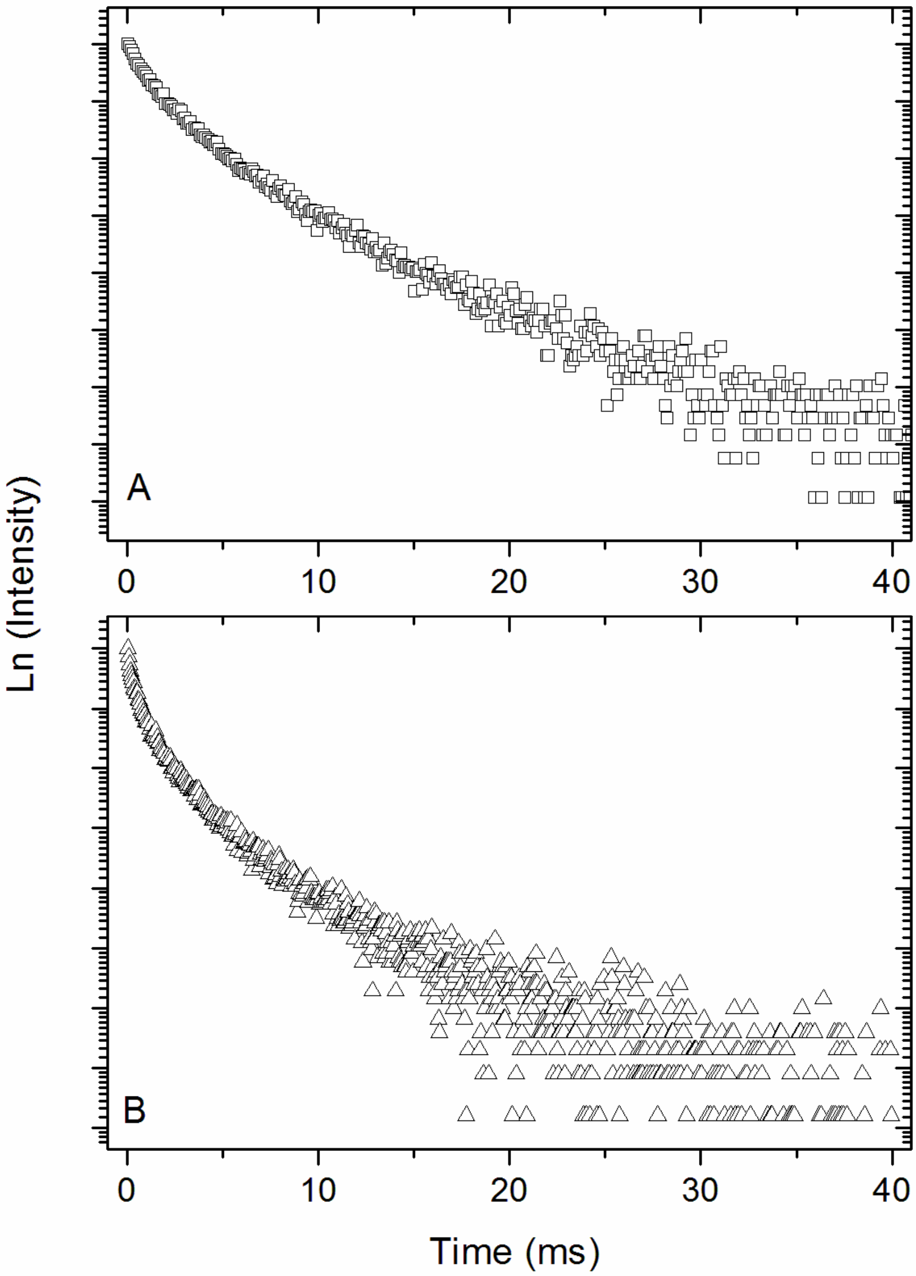

Figure S10. 12K emission decay curves of $[Gd_2(2,3\text{-pzdc})_2(ox)(H_2O)_2]_n$ (**5**), excited at 283 nm and monitored around (A) 520 nm and (B) 450 nm.

Figure S11

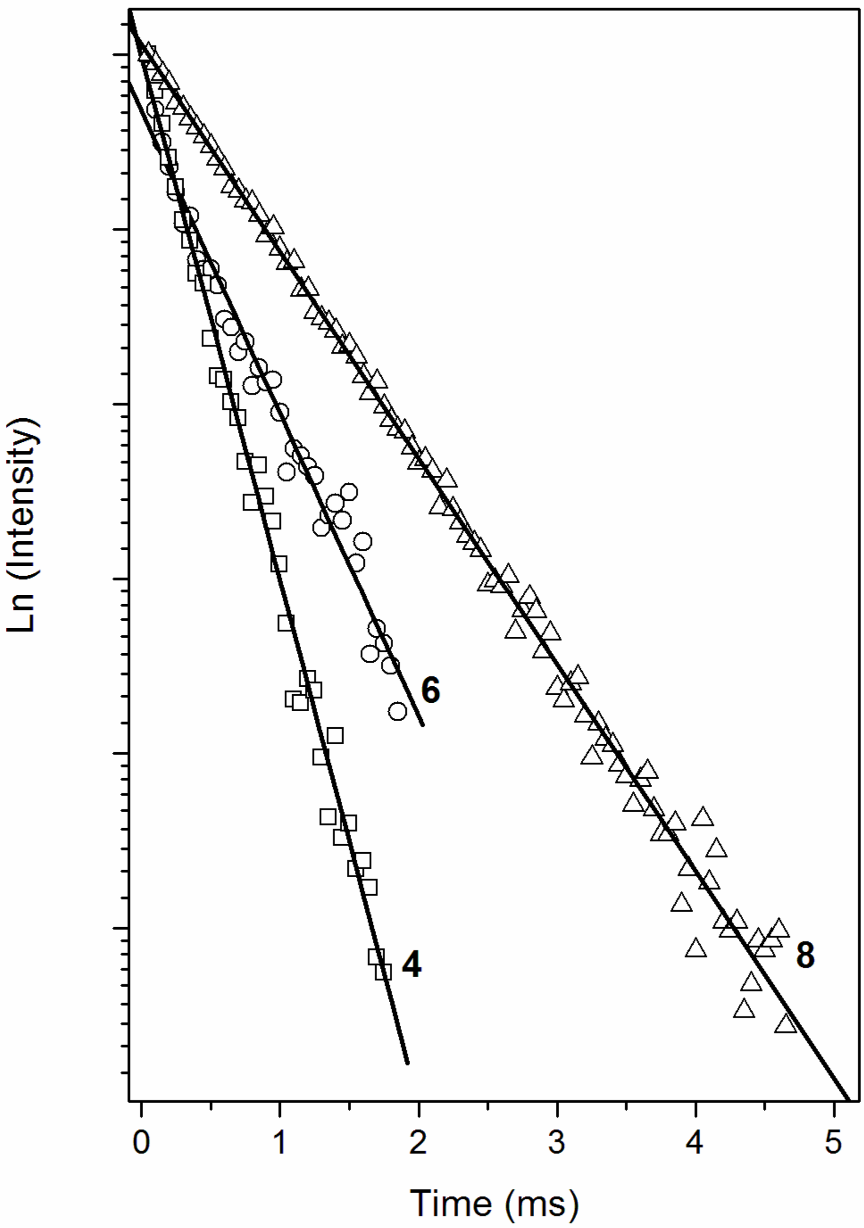

Figure S11. Room temperature emission decay curves of $[Eu_2(2,3\text{-pzdc})_2(ox)(H_2O)_2]_n$ (**4**, □) monitored at 614 nm and excited at 464 nm, of $[Tb_2(2,3\text{-pzdc})_2(ox)(H_2O)_2]_n$ (**6**, ○) monitored at 544 nm and excited at 490 nm, and of $[Tb_2(2\text{-pzc})_4(ox)(H_2O)_6]\cdot 10H_2O$ (**8**, Δ) monitored at 544 nm and excited at 330 nm.